Bright blue emissions on UV-excitation of LaBO₃ (B=In, Ga, Al) perovskite structured phosphors for commercial solid-state lighting applications

B.V. Naveen Kumar [ab], T. Samuel [c], Samatha Bevara [d], K. Ramachandra Rao [e],

Satya Kamal Chirauri [e*] (iD)

a: Department of Physics, Acharya Nagarjuna University, Guntur, India
b: Shri Vishnu College of Engineering for Women(A), Bhimavaram, India
c: GMR Institute of Technology, Rajam, Andhra Pradesh, India
d: Chemistry Division, Vignan's Foundation for Science, Technology and Research, Guntur, Andhra Pradesh, India
e: Crystal Growth & Nanoscience Research Center, Government College (A), Rajahmundry, India
* Corresponding author: satyakamal.ch@gmail.com
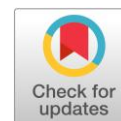
This article belongs to the regular issue.

Abstract

Bright blue photoluminescence (PL) was obtained from Bi^{3+}-activated $LaBO_3$ (B = In, Ga, Al) perovskite nanophosphors. A cost-effective and low-temperature chemical route was employed for preparing Bi^{3+} doped $LaBO_3$ (B=In, Ga, Al) which were then annealed at 1000 ºC. The phase formation, morphological studies and luminescent properties of the as-prepared samples were performed by X-ray diffraction (XRD), scanning electron microscopy (SEM), photoluminescence and optical absorption spectroscopy. Comparison of emission intensities, lifetime studies, energy band gaps and color purity of all samples (pure and Bi^{3+} doped) were investigated for promising applications in UV light-emitting diodes, variable frequency drive (VFD), field emission display (FED), and other photoelectric fields.

1. Introduction

Blue emissive materials have attracted considerable attention because of their vast applications in the fields of sensors, solid-state lighting technology, and light fidelity (Li-Fi) [1–3]. In view of such applications, design and development of blue light-emitting materials is an exciting challenge. Commercially available blue phosphors like GaN and InGaN, in thin-film form, have potential use in bright blue light emitters. Preparation of such nitride materials requires an energy-expensive process and thus hinders the development of cost-effective blue light emitters [4]. Perhaps, in blue light-emitting phosphors, rare-earth ions like Eu^{2+} and Ce^{3+} are commonly used as activator ions, owing to their 4f→5d transitions giving rise to an absorption band ranges in NUV to the blue region and a broad emission band covering blue to the red region [5–8]. However, phosphors doped with Eu^{2+} or Ce^{3+} shows some disadvantage in the view of high cost, high reabsorption and color deviation. Therefore, developing potential luminescent phosphor materials doped with non-rare earth

ions as activators is more promising. Among many recent studies, it was found that Bi^{3+} ion as an activator plays a crucial role in the generation of efficient blue-light emission [9–13]. Alternatively, Bi^{3+} ions with their excited state for electron transition and emission band of Bi^{3+} ion at room temperature can be rationally attributed to the $^3P_1{\rightarrow}^1S_0$ transition, which avoids the reabsorption among phosphors. It is worth mentioning that oxide-based materials are preferred over nitride thin films due to low temperatures and simple methods of preparation. Among many oxides, perovskite materials have been widely investigated for luminescence applications. For example, semiconductor $LaInO_3$ revealed potential properties for the phosphor applications and as a surface for solid oxide fuel cells [14]. Subsequently, $LaAlO_3$ has intensive applications as a substrate for superconductors, magnetic and ferromagnetic thin films and luminescent host materials, and has high thermal stability and good dielectric properties [15–17]. $LaGaO_3$ perovskite has received much attention as a leading host because of its potential use as substrate applications for phosphorus and solid oxide fuel cells [18]. In the last

few years, a considerable amount of research was done on $LaInO_3$, $LaAlO_3$, $LaGaO_3$ perovskite materials. A few research groups have also reported that Bi^{3+} doped $LaInO_3$ and $LaGaO_3$ are efficient blue-emitting luminescent materials. However, to the best of our knowledge, there is no report on the optimization of Bi^{3+} ions in $LaInO_3$, $LaAlO_3$, and $LaGaO_3$ phosphors. Therefore, in this article, we demonstrated a comparative study for bright blue emissions on UV excitation close to industrial standards (colour coordinates: x = 0.15 and y = 0.15) obtained from Bi^{3+} ion doped $LaBO_3$ (B=In, Ga, Al) samples. Hence, from the photo luminescent results, these blue light emitters would be potential materials to increase the efficiency of white light-emitting solid-state devices.

2. Experimental

$La(NO_3)_3 \cdot 6H_2O$ [Merck, Germany], $In(NO_3)_3 \cdot H_2O$ [Sigma-Aldrich, 99.99%], $Al(NO_3)_3 \cdot H_2O$ [Alfa Aesar 99.99%], Gallium(III)nitratehydrate $(Ga(NO_3)_3 \cdot H_2O)$ [Sigma-Aldrich, 99.99%], $Bi(NO_3)_3 \cdot 5H_2O$ [Sigma-Aldrich, 99.99%], were used as starting materials. For the synthesis of pure $LaInO_3$ nanoparticles, stoichiometric amounts of $La(NO_3)_3 \cdot 6H_2O$ and $In(NO_3)_3 \cdot H_2O$ were mixed with 20 ml of distilled water in a two-necked round bottom flask. The solution was slowly stirred and ammonium hydroxide aqueous solution was added dropwise until the clear solution turned intoturbid; then the solution was maintained at 120 °C for 2 hours. The precipitate then formed in the round bottom flask was collected and thoroughly washed five times with methanol and allowed for drying. Later, the samples were heated to 1000 °C at a heating rate of 10 °C per minute in a furnace that maintained the constant temperature for 5 h, then the furnace was turned off and the samples were allowed to settle naturally at room temperature to cool. Finally, the samples were grounded for further investigation. The same procedure was used to prepare $LaInO_3$: 0.5, 1, 2, 2.5, 3 at.% Bi^{3+}, $LaGaO_3$: 1, 1.5, 2, 2.5, 3 at.% Bi^{3+}, $LaAlO_3$: 0.5, 1, 2, 2.5, 3 at.% Bi^{3+} doped nanophosphors, which were also annealed in air at 1000 °C.

3. Results and discussion

3.1. XRD studies

XRD patterns of undoped and selected Bi^{3+} doped $LaInO_3$, $LaGaO_3$ and $LaAlO_3$ samples calcined at 1000 °C are shown
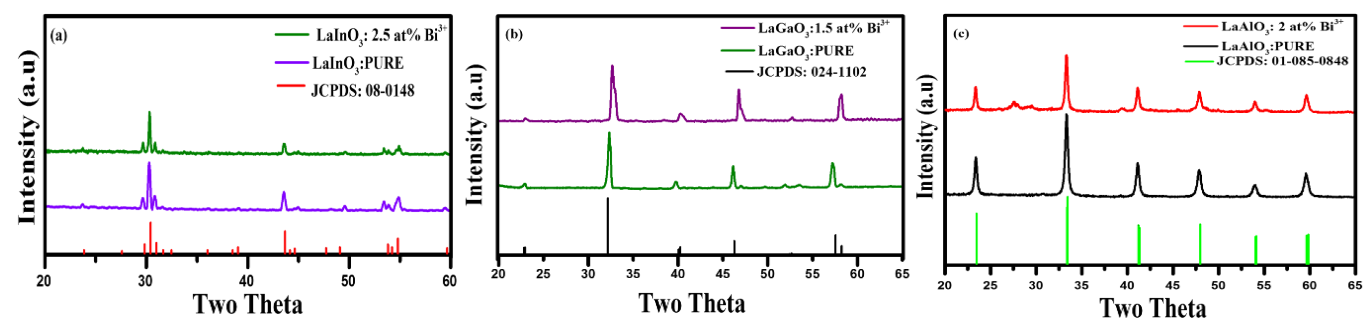
in Fig. 1 (a–c). The diffraction peaks indicate that the calcined samples of $LaInO_3$, $LaGaO_3$ can be indexed in pure orthorhombic phase and $LaAlO_3$ can be indexed in cubic or rhombohedral phase. All diffraction peaks are in good agreement with the previously reported phases of $LaInO_3$, $LaGaO_3$ and $LaAlO_3$ samples, and it is observed that no second phase was detected for the samples indicating that Bi^{3+} was completely dissolved in the host array, which is in good agreement with previously reported literature [19–23]. Typically, the crystal size of the sample is calculated from the Debye–Scherer diffraction line width using the relation d = $0.9\lambda/\beta \cos\theta$, where d is the average crystal size, λ is the X-ray wave length (1.5405 Å), and β is the maximum amplitude, which is correlated to full width at half of the maximum intensity (FWHM) line, and θ is the angle of diffraction.

The average crystal sizes of undoped and doped $LaInO_3$, $LaGaO_3$ and $LaAlO_3$ samples, which were calcined at 1000 °C, are in the range of 90–120 nm. The lattice parameters for both pure and doped $LaInO_3$, $LaGaO_3$ and $LaAlO_3$ were calculated using PowderX software and are listed in Table l.

Table 1 Unit cell parameters of pure and doped $LaInO_3$, $LaGaO_3$ and $LaAlO_3$ samples

Composition	a (Å)	b (Å)	c (Å)	Volume (Å)^3
$LaInO_3$ (JCPDS: 08-0148)	5.7820	8.3360	5.9990	289.14
$LaInO_3$: 2.5 at.% Bi^{3+}	5.7240	8.2450	5.9280	279.76
$LaGaO_3$ (JCPDS: 024-1102)	5.4883	5.5248	7.7499	234.99
$LaGaO_3$: 1.5 at.% Bi^{3+}	5.4963	5.4688	7.7149	231.90
$LaAlO_3$ (JCPDS: 01-085-0848)	3.7860	3.7860	3.7860	54.26
$LaAlO_3$: 2 at.% Bi^{3+}	3.7810	3.7810	3.7810	54.05

3.2. Morphological studies

Fig. 2 (a–f) shows the typical scanning electron microscope (SEM) images of pure and $LaInO_3$: 2.5 at.% Bi^{3+}, $LaGaO_3$: 1.5 at.% Bi^{3+}, $LaAlO_3$: 2 at.% Bi^{3+} doped samples. A collection of crystalline granules and particles was observed in the SEM images of the phosphorus. The SEM images of pure $LaBO_3$ (B = In, Ga, Al) samples are depicted in Fig. 2 (a–c) and Bi^{3+} doped samples in Fig. 2 (d–f). All crystallites are spherical in nature ranging between 90–150 nm.
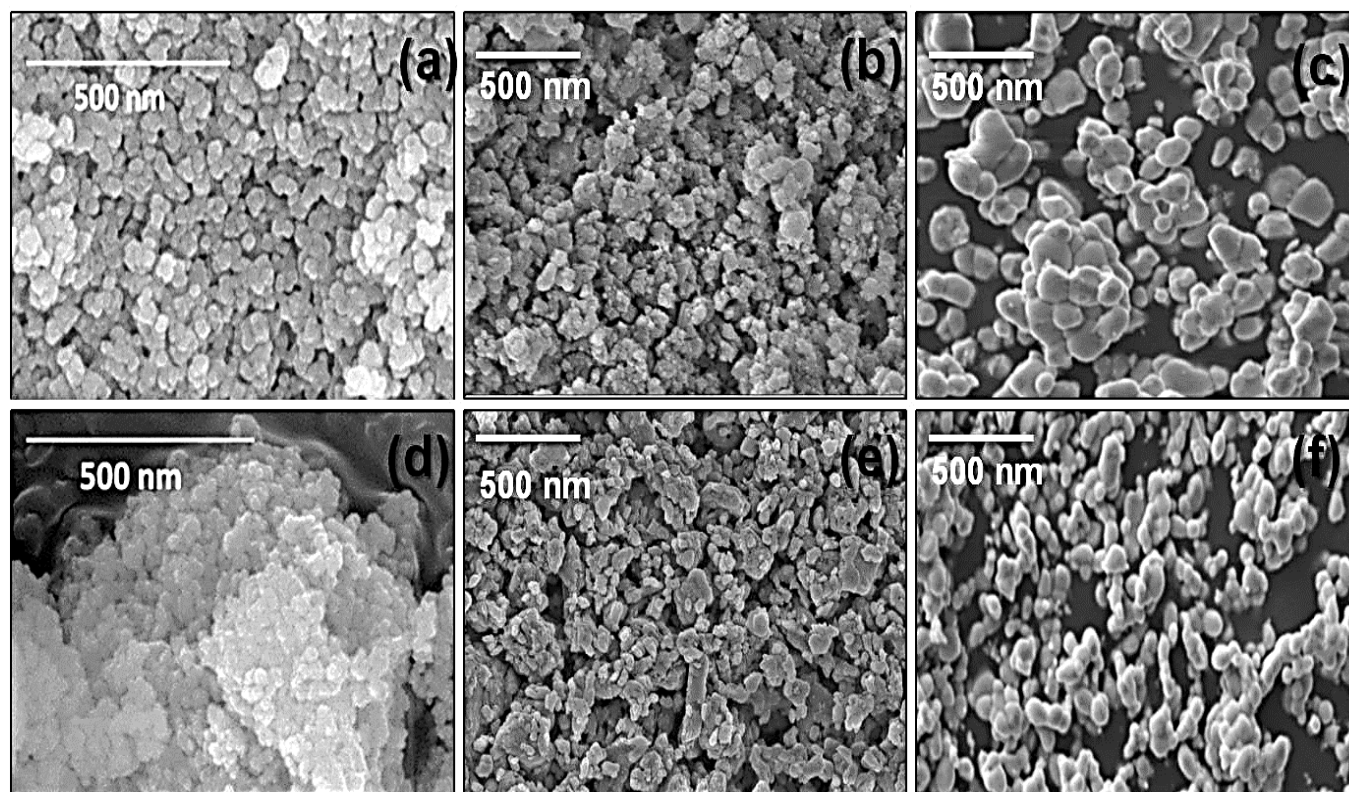

Fig. 1 XRD patterns of pure and Bi^{3+} doped $LaInO_3$ (a), $LaGaO_3$ (b) and $LaAlO_3$ (c) samples calcined at 1000 °C

Fig. 2 SEM images of pure $LaBO_3$ (B = In, Ga, Al) (a–c) and Bi^{3+} doped $LaBO_3$ (B = In, Ga, Al) (d–f) samples

The higher calcinations temperature facilitates the possible rapid arrangement of crystal structure followed by coalescence of particles leading to particle agglomeration causing a considerable reduction in crystallite size of Bi^{3+} doped samples compared to undoped samples. To support this phenomenon, particle size distribution graphs for all the pure and doped samples were calculated using ImageJ software and are presented in Fig. 3 (a–f). The energy dispersive X-ray spectrometer (EDS) spectra used to determine the composition of the samples and show good agreement with the nominal sample compositions (Fig. 4 (a–f)).

3.3. Optical Energy bandgap calculations

Fig. 5 (a–b) shows the plots of $(\alpha h\upsilon)^2$ vs $h\upsilon$ for the as-prepared nanophosphor uses, where α is the optical absorption coefficient and $h\upsilon$ is the energy of the incident photon. The band gap of the optical energy (for example) can be calculated by extending the linear part of the curve $(\alpha h\upsilon)^2 = 0$. Form the plots, it was found that the optical energy bandgaps are equal to 4.16 eV, 5.10 eV and 4.28 eV for $LaInO_3$, $LaGaO_3$ and $LaAlO_3$ pure samples, respectively. The optimum $LaInO_3$: 2.5 at.% Bi^{3+}, $LaGaO_3$: 1.5 at.% Bi^{3+}, $LaAlO_3$: 2 at.% Bi^{3+} doped samples energy bandgap values are 3.81 eV, 4.90 eV and 3.90 eV, respectively. The value of energy gap is reduced considerably on doping with Bi^{3+} ions, which is demonstrated in Fig. 5. Also, it was reported elsewhere that the energy gap of phosphor material decreased in presence of Bi^{3+} ion [24–26]. The Bi^{3+} ion renders some energy levels that have the $6s^2$ valence electrons together to form a continuous band. The decrease in optical energy band gap may result in an increase in the concentration of excited ions in higher energy states. Thus, doping leads to the decrease in the energy of Fermi level and, hence, a reduction in the optical band gap is observed [27].

3.4. Photoluminescence and lifetime decay studies

Emission spectra of $LaInO_3$: 0.5, 1, 2, 2.5, 3 at.% Bi^{3+}, $LaGaO_3$: 1, 1.5, 2, 2.5, 3 at.% Bi^{3+}, $LaAlO_3$: 0.5, 1, 2, 2.5, 3 at.% Bi^{3+} doped samples are shown in Fig. 6 (a–c). All the samples have broad emission bands centered at 432 nm, 373 nm and 350 nm on excitation with 330 nm, 309 nm and 274 nm, respectively, which is attributed to the $^3P_1$–$^1S_0$ transition of Bi^{3+} ions [28]. It was evident that the intensity of the emission band increases as the Bi^{3+} concentration increases, reaching a maximum at 2.5 at.% for $LaInO_3$: Bi^{3+}, 1 at.% for $LaGaO_3$: Bi^{3+} and 2 at.% for $LaAlO_3$: Bi^{3+} samples, and then remarkably decreasing on increasing Bi^{3+} content due to the concentration quenching. The concentration quenching can be triggered because the interactions between two ions increase as doping increases and the decrease in extent of the energy transfer process causes the decrease of the emission intensity [29]. The corresponding excitation spectra, a broad excitation band ranging from 300 to 500 nm with a maximum at about 330, 309, 274 nm, which was arising from $^1S_0$–$^3P_1$ transition of Bi^{3+}, are illustrated in supporting information (Fig. S1). Further, it is noteworthy that in the emission spectra for undoped $LaGaO_3$ a broad band peak maximum at 430 nm is observed, which is due to the GaO_6 octahedral site (Fig. S2). Of all the perovskites from the emission spectra trend, the highest emission intensity is observed for $LaGaO_3$: Bi^{3+} doped samples with a peak position at 375 nm on excitation with 309 nm, which is illustrated in Fig. 6 (b) [30].
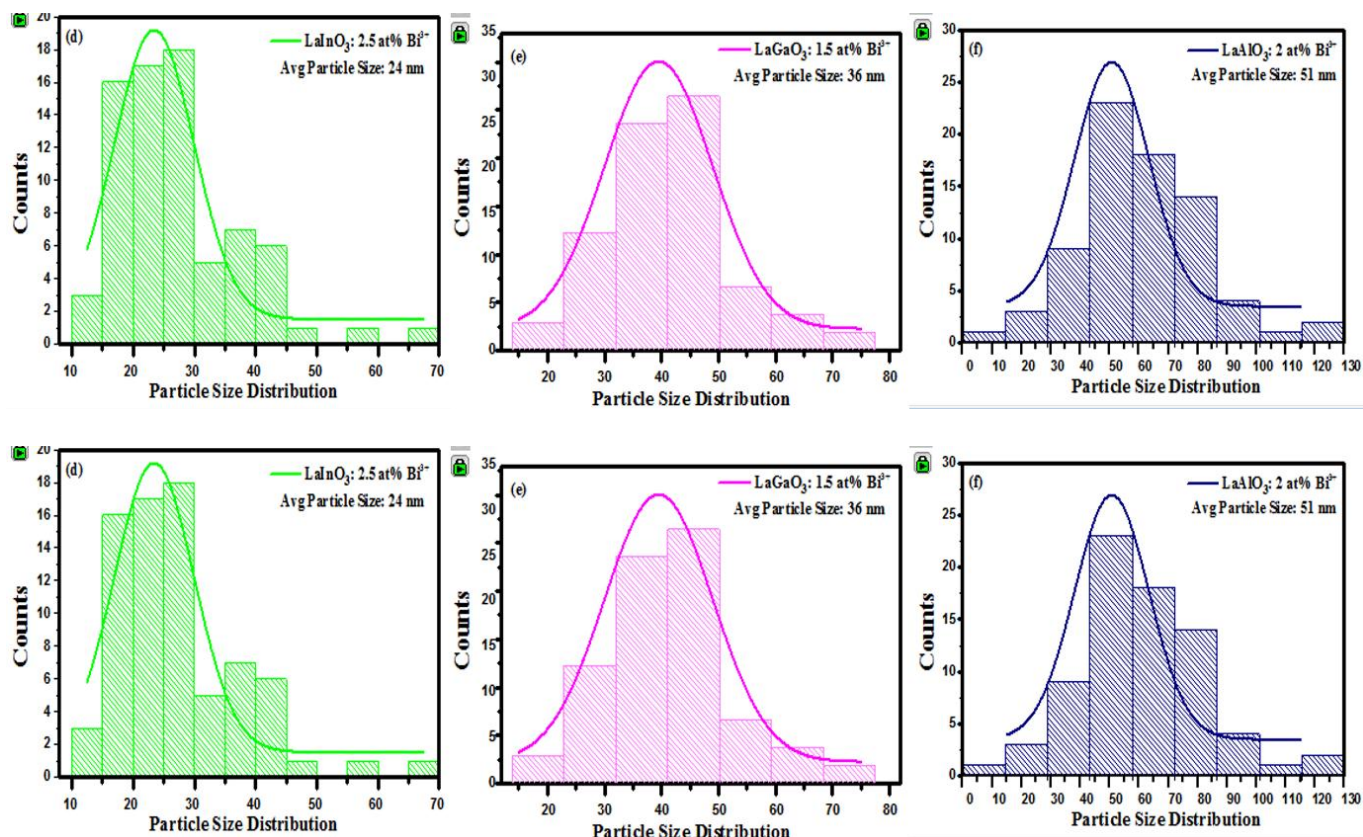
Fig. 3 Particle size distributions of pure $LaBO_3$ (B = In, Ga, Al) (a–) and Bi^{3+} doped $LaBO_3$ (B = In, Ga, Al) (d–f) samples
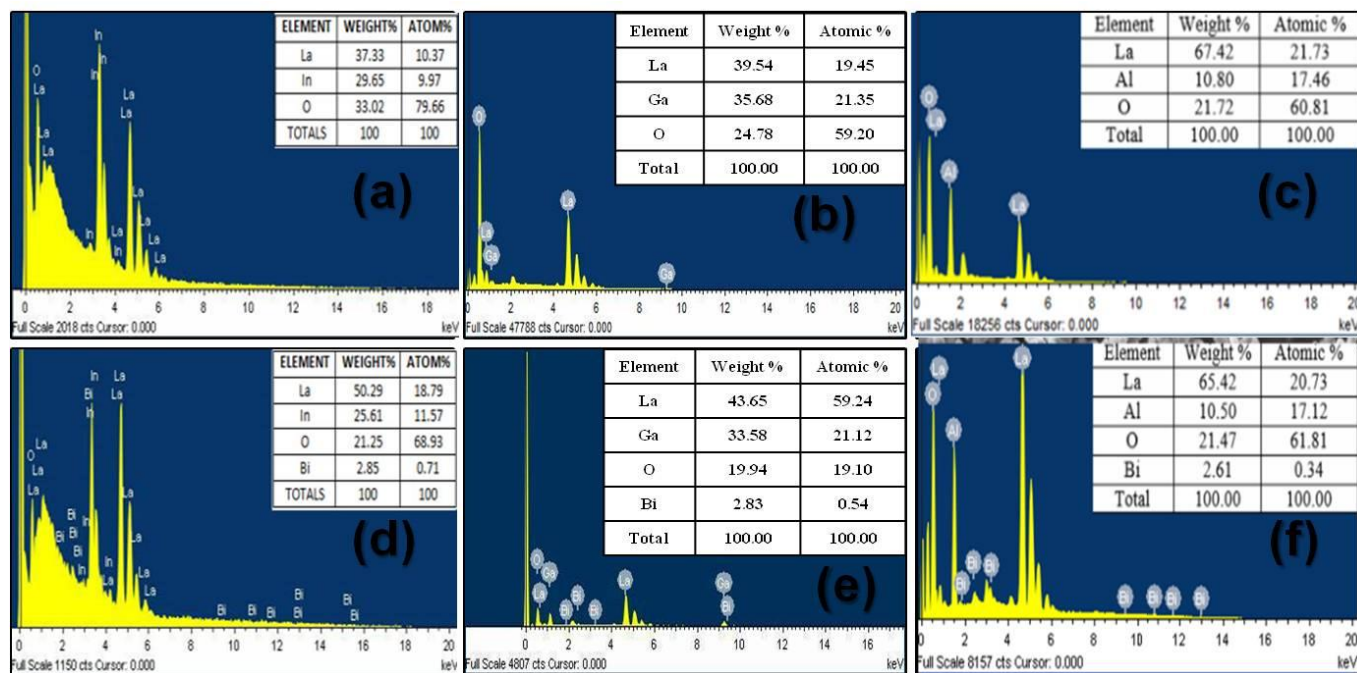

Fig. 4 EDS spectra of pure $LaBO_3$ (B = In, Ga, Al) (a–c) and Bi^{3+} doped $LaBO_3$ (B = In, Ga, Al) (d–f) samples
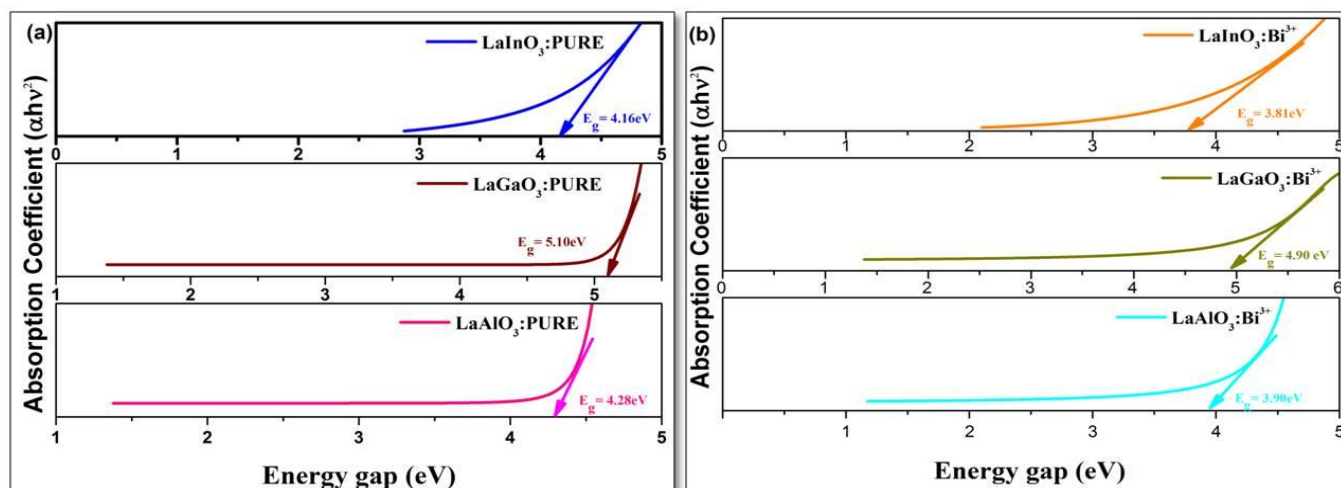
Fig. 5 Optical energy band gaps of pure $LaBO_3$ (B = In, Ga, Al) (a) and Bi^{3+} doped $LaBO_3$ (B = In, Ga, Al) (b) samples
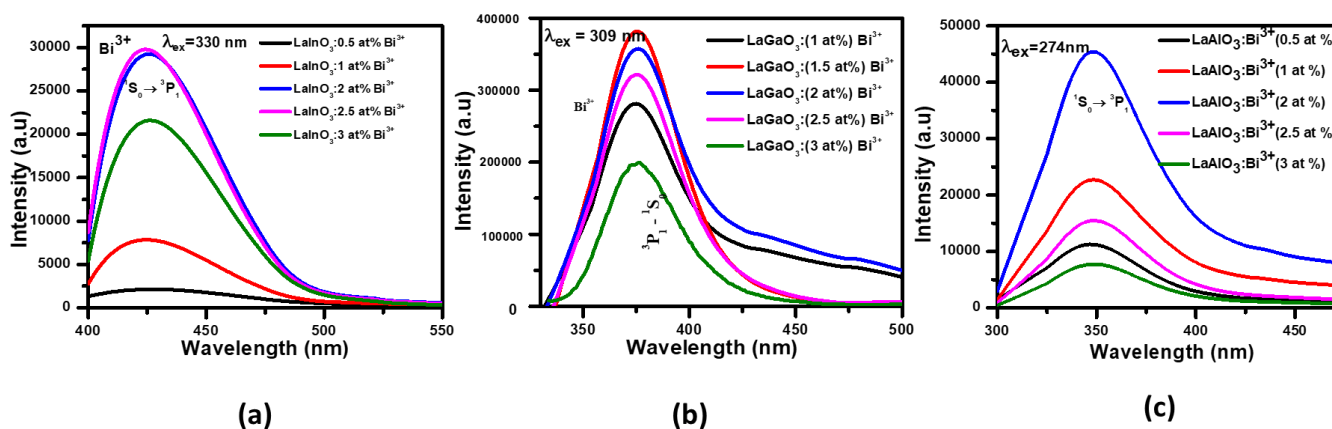

(a)　　　　　　　　　　**(b)**　　　　　　　　　　**(c)**

Fig. 6 Emission spectra of $LaInO_3$: 0.5, 1, 2, 2.5, 3 at.% Bi^{3+} (a), $LaGaO_3$: 0.5, 1, 1.5, 2, 2.5 at.% Bi^{3+} (b) and $LaAlO_3$: 0.5, 1, 2, 2.5, 3 at.% Bi^{3+} (c) doped samples

The reason behind the enhanced intensity from $LaGaO_3:Bi^{3+}$ doped sample is due to the energy transfer phenomena from GaO_6 octahedral sites to Bi^{3+} ions. To confirm this energy transfer, spectral overlap between excitation spectra of $LaGaO_3:Bi^{3+}$ sample and emission spectra of pure $LaGaO_3$ is demonstrated in Fig. 7.

To verify the emission intensity pattern, the corresponding life time decay values (Fig. 8 (a–d)) for the prepared phosphors were calculated according to the following equation:

$$I = A_1 e^{(-t/\tau_1)} + A_2 e^{(-t/\tau_2)}, \qquad (1)$$

where I is the luminescence intensity at the time t, τ_1 and τ_2 are two components of the decay time, A_1 and A_2 are the constants. The average decay times of the samples were found to be 215, 252, 269, 329, 273 ns of $LaInO_3:Bi^{3+}$ (0.5, 1, 2, 2.5, 3 at.% Bi^{3+}), 734 ns, 806 ns and 693 ns of$LaAlO_3$: 0.5, 1, 2, 2.5, 3 at.% Bi^{3+} and for $LaGaO_3$: 1, 1.5, 2, 2.5, 3 at.% Bi^{3+} samples decay life time value was found to be 702 ns and 989 ns, 745 ns, 643 ns and 567 ns, respectively.

3.5. CIE chromatic coordinates

Quantification of the overall emitted colors was done with the help of Commission International De I'Eclairage (CIE) chromaticity coordinates, where any color can be expressed in terms of (x, y) color coordinates, based on emission spectra [31].
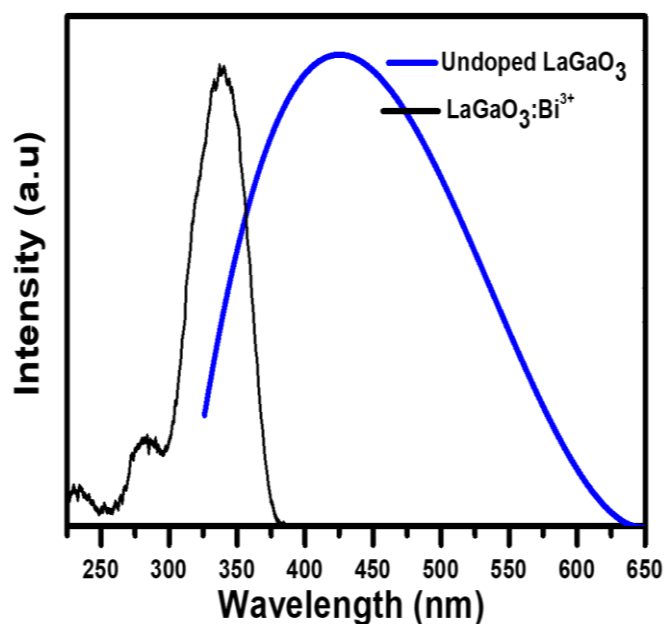

Fig. 7 Spectral overlap of pure and 1.5 at.% Bi^{3+} doped $LaGaO_3$ samples

Fig. 9 (a–c) represents the CIE coordinates of LaInO$_3$, LaGaO$_3$ and LaAlO$_3$ as-prepared samples doped with Bi^{3+}. The CIE diagram of LaInO$_3$: 3 at.% Bi^{3+} lies in bright BLUE [Points (0.22, 0.18)], LaGaO$_3$: 1 at.% Bi^{3+} lies in BLUE [Points (0.18, 0.15)] and LaAlO$_3$: 1 at.% Bi^{3+} lies in BLUE [Points (0.26, 0.22)]. From the color coordinators, it is evident that LaInO$_3$, LaAlO$_3$ lies in nearly blue regions, whereas LaGaO$_3$ samples lie in the BLUE region. So, from color purity analysis, the coordinates of LaGaO$_3$: 1 at.% Bi^{3+} lies very near to the industrial standard blue emission coordinates, i.e. (0.15, 0.15).

4. Conclusions

All the samples were prepared by a cost-effective and low-temperature polyol route method and were heated to 1000 ºC. From the XRD patterns and SEM, it was observed that all samples range in nanoscale in agreement with the reported data. From PL studies, it was evident that all the emission peaks of as-prepared samples are attributed to $^3P_1$–$^1S_0$ transition of Bi^{3+} ions emitting strong bright blue luminescence. When excited by UV light, LaGaO$_3$ (pure and Bi^{3+}) samples shows emissions. The emissions from the pure sample of LaGaO$_3$ indicates that the host lattice itself is optically self-activated, whereas when the host lattice is

doped with Bi^{3+} the intensity of emissions are enhanced. This is beneficial for the development of optically self-activated lighting devices. From the emission spectra and the data plotted for CIE coordinates, out of all three samples, LaGaO$_3$: 1 at.% Bi^{3+} CIE coordinates nearly meets the standard blue emission coordinates i.e. (0.15, 0.15). Thus, in comparison with the other samples, we finally conclude that LaGaO$_3$: 1 at.% Bi^{3+} would be the best blue light-emitting phosphor that may be potentially used in solid-state lighting applications.

Acknowledgements

Conflict of interest

The authors declare that they have no known competing financial interests or personal relationships that could have appeared to influence the work reported in this paper.
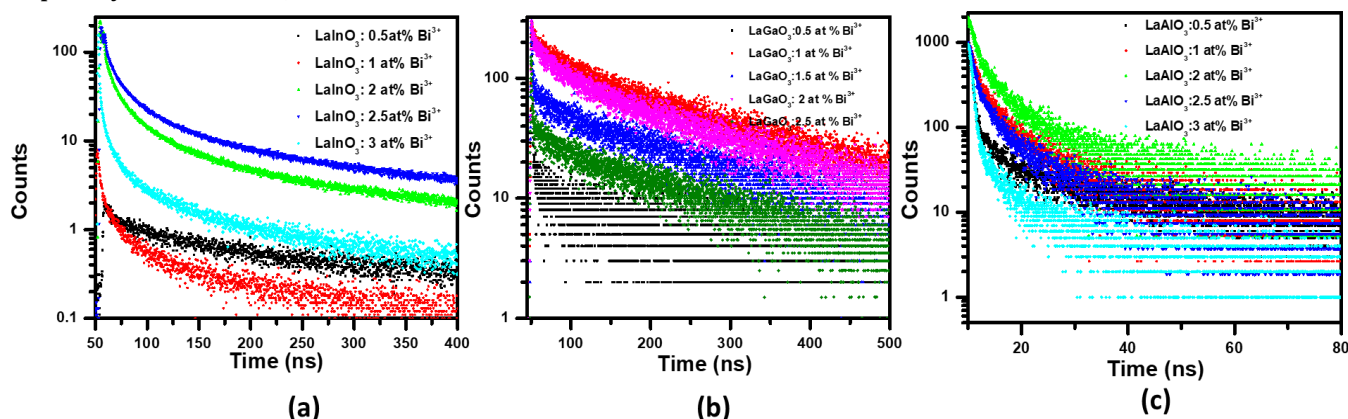

Fig. 8 Life time decay curves of LaInO$_3$:Bi^{3+} (a), LaGaO$_3$:Bi^{3+} (b), and LaAlO$_3$:Bi^{3+} (c) doped samples
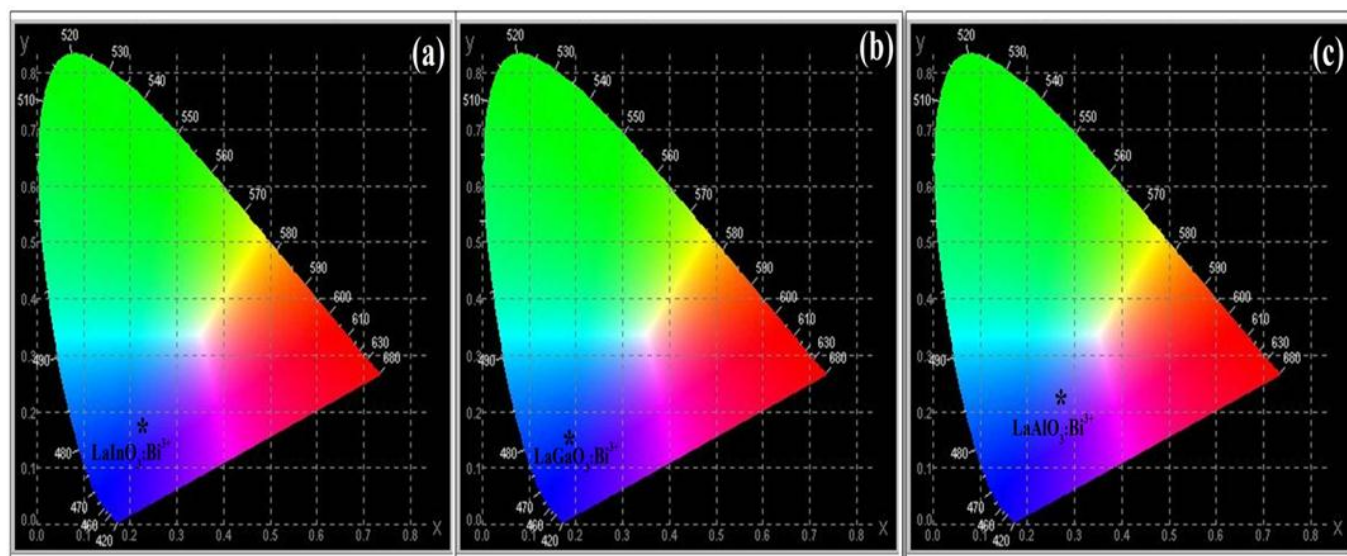

Fig. 9 CIE chromatic coordinates of LaInO$_3$ (a), LaGaO$_3$ (b) and LaAlO$_3$ (c) samples doped with Bi^{3+}

References

1. Ferreira RX, Xie E, McKendry JJ, Rajbhandari S, Chun H, Faulkner G, et al. High bandwidth GaN-based micro-LEDs for multi-Gb/s visible light communications. IEEE Photonics Technol Lett. 2016;28(19):2023–2026. doi:10.1109/LPT.2016.2581318

2. Peng S, Zhao Y, Fu C, Pu X, Zhou L, Huang Y, et al. Acquiring high-performance deep-blue OLED emitters through an unexpected blue shift color-tuning effect induced by electron-donating-OMe substituents. Chem Eur J. 2018;24(32):8056–8060. doi:10.1002/chem.201800974

3. De J, Yang W-Y, Bala I, Gupta SP, Yadav RAK, Dubey DK, et al. Room-temperature columnar liquid crystals as efficient pure deep-blue emitters in organic light-emitting diodes with an external quantum efficiency of 4.0%. ACS Appl Mater Interfaces. 2019;11(8):8291–8300. doi:10.1021/acsami.8b18749

4. Nakamura S. Background story of the invention of efficient InGaN blue-light-emitting diodes (Nobel Lecture). Angewandte Chem Int Edition. 2015;54(27):7770–7788. doi:10.1002/anie.201500591

5. Wang C-Y, Takeda T, Ten Kate OM, Tansho M, Deguchi K, Takahashi K, et al. Ce-doped $La_3Si_{6.5}Al_{1.5}N_{9.5}O_{5.5}$, a rare highly efficient blue-emitting phosphor at short wavelength toward high color rendering white LED application. ACS Appl Mater Interfaces. 2017;9(27):22665–22675. doi:10.1021/acsami.7b03909

6. Zhang J, Zhang J, Zhou W, Ji X, Ma W, Qiu Z, et al. Composition screening in blue-emitting $Li_4Sr_{1+x}Ca_{0.97-x}(SiO_4)_2$: Ce^{3+} phosphors for high quantum efficiency and thermally stable photoluminescence. ACS Appl Mater Interfaces. 2017;9(36):30746–30754. doi:10.1021/acsami.7b08671

7. Pawade V, Dhoble S. Novel blue-emitting $SrMg_2Al_{16}O_{27}$:Eu^{2+} phosphor for solid-state lighting. Lumin. 2011;26(6):722–727. doi:10.1002/bio.1304

8. Li G, Tian Y, Zhao Y, Lin J. Recent progress in luminescence tuning of Ce^{3+} and Eu^{2+}-activated phosphors for pc-WLEDs. Chem Soc Rev. 2015;44(23):8688–8713. doi:10.1039/C4CS00446A

9. Han J, Pan F, Molokeev MS, Dai J, Peng M, Zhou W, et al. Redefinition of crystal structure and Bi^{3+} yellow luminescence with strong near-ultraviolet excitation in La_3BWO_9:Bi^{3+} phosphor for white light-emitting diodes. ACS Appl Mater Interfaces. 2018;10(16):13660–13668. doi:10.1021/acsami.8b00808

10. Sun W, Li H, Zheng B, Pang R, Jiang L, Zhang S, et al. Electronic structure and photoluminescence properties of a novel single-phased color tunable phosphor $KAlGeO_4$:Bi^{3+}, Eu^{3+} for WLEDs. J Alloys Compd. 2019;774:477–486. doi:10.1016/j.jallcom.2018.10.087

11. Li H, Pang R, Liu G, Sun W, Li D, Jiang L, et al. Synthesis and luminescence properties of Bi^{3+}-activated K_2MgGeO_4: a promising high-brightness orange-emitting phosphor for WLEDs conversion. Inorganic Chem. 2018;57(19):12303–12311. doi:10.1021/acs.inorgchem.8b02025

12. Jiang Z, Gou J, Min Y, Huang C, Lv W, Yu X, et al. Crystal structure and luminescence properties of a novel non-rare-earth activated blue-emitting garnet phosphor $Ca_4ZrGe_3O_{12}$: Bi^{3+} for n-UV pumped light-emitting diodes. J Alloys Compd. 2017;727:63–68. doi:10.1016/j.jallcom.2017.08.109

13. Li H, Pang R, Luo Y, Wu H, Zhang S, Jiang L, et al. Structural micromodulation on Bi^{3+}-doped $Ba_2Ga_2GeO_7$ phosphor with considerable tunability of the defect-oriented optical properties. ACS Appl Electron Mater. 2019;1(2):229–237. doi:10.1021/acsaelm.8b00072

14. Valange S, Beauchaud A, Barrault J, Gabelica Z, Daturi M, Can F. Lanthanum oxides for the selective synthesis of phytosterol esters: correlation between catalytic and acid–base properties. J Catalysis. 2007;251(1):113–122. doi:10.1016/j.jcat.2007.07.004

15. Onishi Y, Nakamura T, Adachi S. Solubility limit and luminescence properties of Eu^{3+} ions in Al_2O_3 powder. J Lumin. 2016;176:266–271. doi:10.1016/j.jlumin.2016.03.030

16. Mann CK, Mann CK, Vickers TJ, Gulick WM. Instrumental analysis: HarperCollins Publishers; 1974.

17. Michalet X, Pinaud F, Lacoste TD, Dahan M, Bruchez MP, Alivisatos AP, et al. Properties of fluorescent semiconductor nanocrystals and their application to biological labeling. Single Mol. 2001;2(4):261–276. doi:10.1002/1438-5171(200112)2:4<261::AID-SIMO261>3.0.CO;2-P

18. Yoffe AD. Semiconductor quantum dots and related systems: electronic, optical, luminescence and related properties of low dimensional systems. Adv Phys. 2001;50(1):1–208. doi:10.1080/00018730010006608

19. Yu M, Lin J, Zhou Y, Wang S. Citrate–gel synthesis and luminescent properties of $ZnGa_2O_4$ doped with Mn^{2+} and Eu^{3+}. Mater Lett. 2002;56(6):1007–1013. doi:10.1016/S0167-577X(02)00664-X

20. Babu KE, Murali N, Babu KV, Shibeshi PT, Veeraiah V. Investigation of optoelectronic properties of cubic perovskite $LaGaO_3$. AIP Conf Proceed. 2014. doi:10.1063/1.4898236

21. Yang HK, Oh JH, Moon BK, Jeong JH, Yi SS. Photoluminescent properties of near-infrared excited blue emission in Yb, Tm co-doped $LaGaO_3$ phosphors. Ceram Int. 2014;40(8):13357–13361. doi:10.1016/j.ceramint.2014.05.051

22. Jacquier B, Boulon G, Sallavuard G, Gaume-Mahn F. Bi^{3+} center in a lanthanum gallate phosphor. J Solid State Chem. 1972;4(3):374–378. doi:10.1016/0022-4596(72)90152-1

23. Porter-Chapman Y, Bourret-Courchesne E, Derenzo SE. Bi^{3+} luminescence in $ABiO_2Cl$ (A = Sr, Ba) and $BaBiO_2Br$. J Lumin. 2008;128(1):87–91. doi:10.1016/j.jlumin.2007.05.007

24. Weigel M, Middel W, Blasse G. Influence of ns^2 ions on the luminescence of niobates and tantalates. J Mater Chem. 1995, 5, 981–983. doi:10.1039/JM9950500981

25. Yadav RS, Rai SB. Surface analysis and enhanced photoluminescence via Bi^{3+} doping in a Tb^{3+} doped Y_2O_3 nano-phosphor under UV excitation. J Alloys Compd. 2017;700:228–237. doi:10.1016/j.jallcom.2017.01.074

26. Shaik EB, Kamal CS, Srinivasu K, et al. Optical insights of indium-doped $\beta–Ga_2O_3$ nanoparticles and its luminescence mechanism. J Mater Sci Mater Electron. 2020;31:6185–6191. doi:10.1007/s10854-020-03171-7

27. Erkişi A, Gökoğlu G, Sürücü G, Ellialtıoğlu R, Yıldırım EK. First-principles investigation of $LaGaO_3$ and $LaInO_3$ lanthanum perovskite oxides. Philosoph Mag. 2016;96(19):2040–2058. doi:10.1080/14786435.2016.1189100

28. Srivastava AM. Luminescence of Bi^{3+} in $LaGaO_3$. Mater Res Bull. 1999;34(9):1391–1396. doi:10.1016/S0025-5408(99)00149-X

29. He H, Huang X, Chen L. Sr-doped $LaInO_3$ and its possible application in a single layer SOFC. Solid State Ionics. 2000;130(3–4):183–193. doi:10.1016/S0167-2738(00)00666-4

30. Ruiz-Trejo E, Tavizon G, Arroyo-Landeros A. Structure, point defects and ion migration in $LaInO_3$. J Phys Chem Solids. 2003;64(3):515–521. doi:10.1016/S0022-3697(02)00358-X

31. Blasse G, Bril A. Crystal structure and fluorescence of some lanthanide gallium borates. J Inorg Nucl Chem. 1967;29(1):266–267.